Decreasing Water Activity by Tetrahydrofuran Electrolyte Additive for Highly Reversible Aqueous Zinc Metal Batteries

Wei He ¹, Yao Ren ³, Buddhi Sagar Lamsal ¹, Jyotshna Pokharel ¹, Kena Zhang ³, Parashu Kharel ⁴, James J. Wu ⁵, Xiaojun Xian ¹, Ye Cao ^{3, *}, Yue Zhou ^{2, *}

- ¹ Department of Electrical Engineering and Computer Science, South Dakota State University, Brookings, SD 57007, USA
- ² Department of Mechanical Engineering, The University of Texas at Dallas, 800 W Campbell Rd, Richardson, TX 75080, USA
- ³ Department of Materials Science and Engineering, University of Texas at Arlington, Arlington, TX 76019, USA
- ⁴ Department of Physics, South Dakota State University, Brookings, SD 57007, USA
- ⁵ NASA Glenn Research Center, Cleveland, OH 44135, USA
- $*Corresponding\ Author:\ E-mail\ address:\ ye.cao@uta.edu;\ zhou@utdallas.edu$

Abstract

Aqueous zinc metal batteries show great promise in large-scale energy storage. However, the decomposition of water molecules leads to severe side reactions, resulting in the limited lifespan of Zn batteries. Here, the tetrahydrofuran (THF) additive was introduced into the zinc sulfate (ZnSO₄) electrolyte to reduce the water activity by modulating the solvation structure of the Zn hydration layer. The tetrahydrofuran molecule can play as a proton acceptor to form hydrogen bonds with water molecules, which can prevent water-induced undesired reactions. Thus, in an optimal 2M ZnSO₄/THF (5% by volume) electrolyte, the hydrogen evolution reaction (HER) and by-products precipitation can be suppressed, which greatly improves the cycling stability and Coulombic efficiency of reversible Zn plating/stripping. The Zn symmetrical cells exhibit ultralong working cycles with a wide range of current density and capacity. The THF additive also enables a high Coulombic efficiency in the Zn||Cu cell with an average value of 99.59% over 400 cycles and a high reversible capacity with a capacity retention of 97.56% after 250 cycles in Zn||MnO₂ full cells. This work offers an effective strategy with high scalability and low cost for the protection of Zn metals electrodes in aqueous rechargeable batteries.

Keywords: aqueous zinc metal batteries, zinc anode, tetrahydrofuran, HER, hydrogen bonds

1. Introduction

Zinc metal is a promising anode material because of its high theoretical capacity (5855 mAh mL⁻¹ and 820 mAh g⁻¹) and low redox potential (-0.76 V versus the standard hydrogen electrode, SHE).¹⁻⁴ Moreover, zinc's abundance and availability on earth, and its compatibility with non-flammable aqueous electrolytes make zinc batteries safe, environmentally friendly, and cost-effective.⁵⁻⁶ Therefore, aqueous zinc metal batteries (AZMBs) are considered as an alternative to lithium-ion batteries in large-scale energy storage.⁷⁻⁸ However, AZMBs suffer from electrode corrosion, poor Coulombic efficiency (CE), and dendrite growth during cycling, resulting in limited cycle life.⁹⁻¹⁰ These challenges stem from the interaction between Zn metal and the aqueous electrolytes, which causes the decomposition of water to generate H₂ and produce an inactive by-products on the surface of the Zn electrode.¹¹⁻¹²

To restrain the reactivity of water molecules, various strategies have been proposed by adjusting the composition of the electrolyte to form a highly coordinated solvation sheath. ¹³⁻¹⁶ Water-in-salt electrolytes (WISEs) with a high molality can reduce the reactivity of water molecules and extend the electrochemical stability window. ¹⁷⁻¹⁸ Thus, the WISEs can improve the cycling stability and boost Zn electrode reversibility. For example, Gao et al. reported a record super-solubility ZnCl₂/ZnBr₂/Zn(OAc)₂ aqueous electrolyte with a high molality of 75 m attributed to the formation of acetate-capped water-salt oligomers bridged by Br⁻/Cl⁻-H and Br⁻/Cl⁻/O-Zn²⁺ interactions. ¹⁹ This super soluble electrolyte enabled a high reversible capacity and a good Coulombic efficiency. However, accompanied by favorable electrochemical behaviors, the WISEs would also cause high cost and high viscosity, resulting in the application being held up. Introducing organic additives in the aqueous electrolytes is another approach to reduce water activity. ¹³ Some small organic molecules can partially replace the water molecule in

the solvation sheath to mitigate the water decomposition during cycling.^{1, 20-22} Wang's group developed a dilute electrolyte by adding dimethyl sulfoxide (DMSO) to suppress water reduction and Zn dendrite growth.¹⁴ The findings showed that DMSO replaces the H₂O in Zn²⁺ solvation sheath to form strong H₂O-DMSO interaction, inhibiting the decomposition of solvated H₂O. However, the fundamental effect of the organic additive on the stability of the interface between the Zn electrode and the aqueous electrolyte is still clusive. Thus, it is necessary to develop newtype organic additives with low cost and high scalability to address issues of AZMBs with new mechanisms. Among organic chemicals, cyclic ethers such as 1,3-dioxane and THF are widely used in various chemical fields as a solvent.²³ These cyclic ethers are miscible with H₂O at any composition and their solvent properties such as dielectric constant and viscosity can be adjusted by changing the mixing molar ratio.²⁴ The cyclic ether molecules can play as a proton acceptor to form hydrogen bonds between the oxygen atoms of the cyclic ether molecules and protons of water molecules.²⁵

Herein, for the first time, a common organic compound of THF was introduced into the 2M ZnSO₄ electrolyte. The THF as a proton acceptor can moderately disrupt the water network by forming hydrogen bonds to decrease the water activity, thus optimizes the solvation structure of the Zn hydration layer to suppress the decomposition of water and the generation of by-products. Therefore, the Zn metal anode showed an improved electrochemical behavior in the 2M ZnSO₄ electrolyte with a small amount of THF (5% by volume). The Zn symmetrical cell delivered an ultralong lifespan of 1300 hours at 0.5 mA cm⁻² and 0.5 mAh cm⁻². A stable CE in Zn||Cu asymmetrical cell is achieved over 430 cycles with a high average value of 99.59%, showing an exceptional Zn plating/stripping reversibility. Additionally, the THF additive in the ZnSO₄

electrolyte also enhances the cycling performance of the Zn-ion full cell with Zn metal as anode and MnO_2 as the cathode.

2. Experimental Section

- **2.1. Materials.** Zinc (Zn) foil with a thickness of 0.08 mm, tetrahydrofuran (THF), titanium (Ti) foil, copper (Cu) foil, ZnSO₄·7H₂O, MnSO₄·H₂O, KMnO₄, were purchased from Sigma-Aldrich. Carbon paper (TGP-H-090 with 5% wet proofing) was bought from the Fuel Cell Earth. Glass fiber (GB-100R) was produced by Toyo Roshi Kaisha, Ltd.
- 2.2. Preparation of the Electrolyte and Electrode. To prepare the baseline 2M ZnSO₄ electrolyte, 11.5 g ZnSO₄·7H₂O was dissolved in 14.96 mL deionized water. For THF-based electrolytes, different amounts of THF were added and volume ratios of THF in the solvent are 2.5%, 5%, 7.5%, and 10%, respectively. The relevant electrolytes were denoted as 2M ZnSO₄/THF 2.5%, 2M ZnSO₄/THF 5%, 2M ZnSO₄/THF 7.5% and 2M ZnSO₄/THF 10%. The cathode material of MnO₂ was prepared by a hydrothermal method according to the reference. The MnO₂ electrode was prepared by mixing MnO₂ powder, polyvinylidene fluoride (PVDF), and carbon black (Super-P) in N-Methyl-2-pyrrolidone (NMP) with a weight ratio of 8: 1: 1. After stirring for 24 hours, the homogeneous slurry was cast uniformly on the carbon paper. After being dried in vacuum oven overnight at 100 °C, the MnO₂ electrode was punched into 12 mm circular discs.
- **2.3. Structural Characterization**. The XRD was conducted by a Rigaku SmartLab diffractometer, and the Raman spectrum was carried out by LabRAM HR (HORIBA, 532 nm UV laser). The morphology characterization (SEM, EDS elemental mapping) was performed using scanning electron microscopy (SEM, Hitachi, S-3400 and S-4700). FTIR spectra were

recorded on an infrared instrument of Nicolet 6700 (Thermo Scientific). The contact angle was measured by the VCA2000 video contact angle system. For the in-situ optical observation, the Nikon Eclipse TS2 optical microscope was used.

2.4. Electrochemical Characterization: For Zn symmetrical cell test, the CR-2035 cell was assembled in the air with two Zn chips with a diameter of 12 mm, 100 μL electrolyte, and glass fiber as a separator. Coulombic efficiency (CE) was measured in Zn||Cu cell with Cu foil as the counter electrode, performed at 1 mA cm⁻² with a capacity of 1 mAh cm⁻². For Zn||MnO₂ full cell, the cell was assembled into CR-2035-type cells in the air with a zinc chip as the counter electrode. 0.1 M MnSO₄, which can balance the dissolution loss of MnO₂, was added to the electrolytes. The galvanostatic Zn plating/stripping in the Zn symmetrical cell, Zn||Cu half-cell, and Zn||MnO₂ full cell were tested by a Neware CT-4008 battery-testing system. The cyclic voltammetry (CV), electrochemical impedance spectroscopy (EIS), linear polarization, and chronoamperograms (CAs) measurements were carried out on an electrochemical workstation (Bio-Logic SAS). Details of the computational methods are described in the Supporting Information.

3. Results and Discussion

3.1. DFT Simulation and Electrolyte Characterization

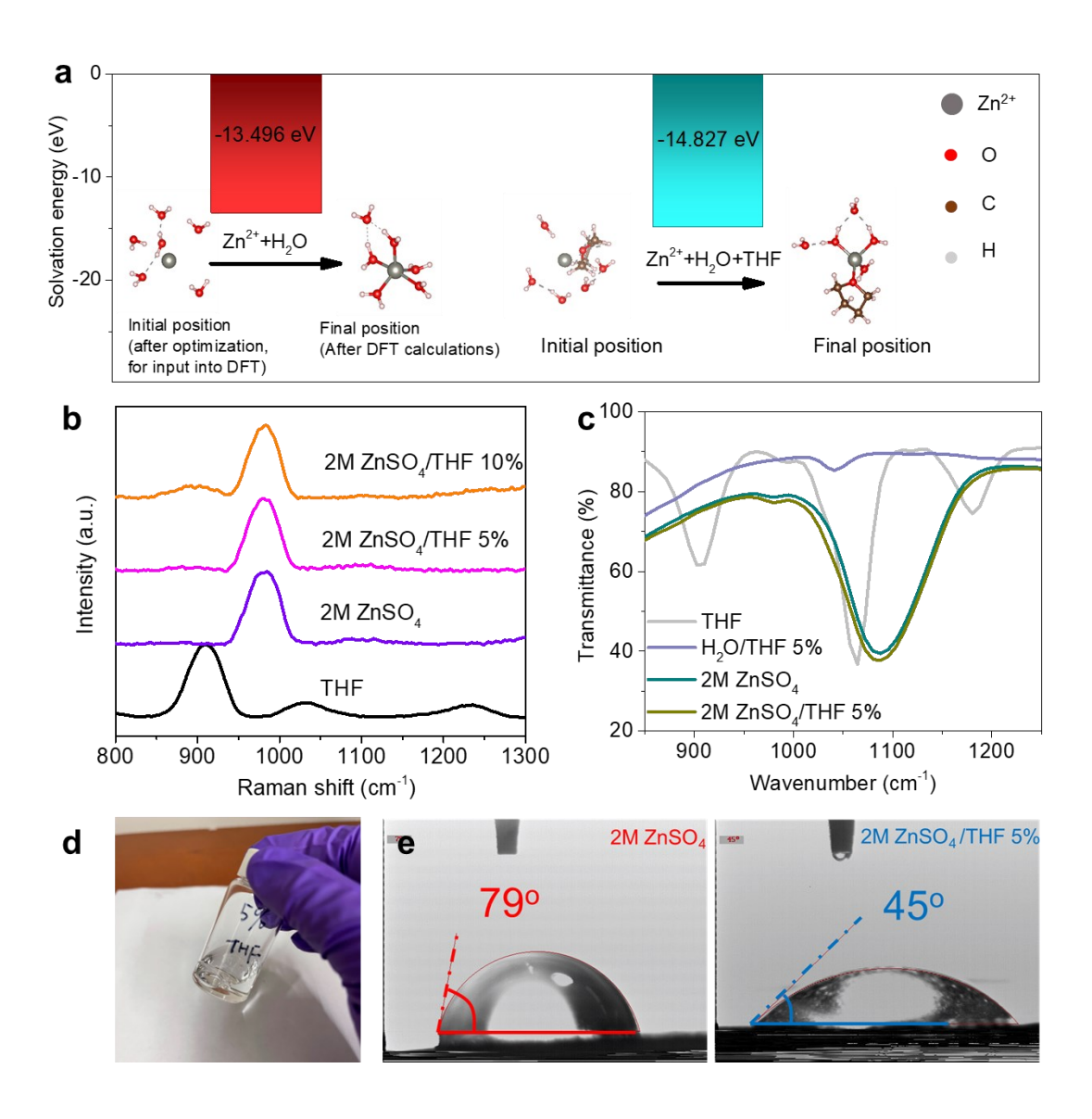


Figure 1. Structures and properties of the baseline 2M ZnSO₄ and 2M ZnSO₄/THF 5% electrolytes.

(a) The optimized solvation structure and corresponding solvation energy with THF additive in DFT calculations. (b) Raman spectra. (c) FTIR spectra. (d) Digital photography of the 2M ZnSO4 /THF 5% electrolyte after setting aside for 30 days. (e) Contact angle measurement of different electrolytes on Zn electrode.

To prepare the desired electrolytes, the ZnSO₄ salt was dissolved in the mixture of H₂O/THF solvent with different volume ratios. Figure S1 shows the molecular formula of water and THF molecules, where THF has one oxygen atom as a proton acceptor within the molecule. Thus, the oxygen atoms within THF can form hydrogen bonds with protons of water molecules to decrease the water activity. DFT simulations are performed to study the Zn²⁺ solvation energy in the aqueous electrolytes. Zn²⁺ is considered to mainly coordinate with 6 H₂O molecules (Zn[H₂O]₆²⁺) in the low concentration ZnSO₄ electrolyte based on the previous references.²⁶⁻²⁷ With the introduction of the THF additive, some THF molecules will replace water molecules in the main Zn[H₂O]₆²⁺ solvation structure due to the strong interaction between THF and water by the hydrogen bond. Many possible solvation configurations of Zn[H₂O]_x[THF]_y²⁺ emerge in the optimized 2M ZnSO₄/THF 5% electrolyte. Because the ratio of water molecules and THF molecules is larger than 5:1, the possible solvation structure with THF molecules is that one THF molecule replaces one water molecule in the Zn[H₂O]₆²⁺ solvation structure to form Zn[H₂O]₅[THF]²⁺. Thus, the representative solvation structures of Zn²⁺ in two different electrolytes mentioned above are shown in Figure 1a. First, the total energy (E_{total}) of $Zn[H_2O]_6^{2+}$ and $Zn[H_2O]_5[THF]^{2+}$ solvation structures are calculated. The, E_{H_2O} and E_{THF+H_2O} are calculated by removing the Zn²⁺ ion from the two solvation structures. Meanwhile, the energy of a single ${\rm Zn^{2^+}}$ ion ($E_{{\rm Zn^{2^+}}}$) is also calculated separately. Finally, the solvation energy ($E_{\rm sol}$) is calculated as the difference between E_{total} , $E_{H_2O/THF+H_2O}$ and $E_{Zn^{2+}}$ (Supplementary, Equation 1). These results are summarized in Figure 1a and Table S1. It is found that the solvation energy of Zn[H₂O]₆²⁺ is calculated to be -13.496 eV, which agrees with the values in the previous literature.²⁸ On the other hand, the solvation energy of Zn[H₂O]₅[THF]²⁺ is -14.827 eV, which is

1.331 eV lower than that of $Zn[H_2O]_6^{2^+}$, indicating that $Zn[H_2O]_5[THF]^{2^+}$ is a more stable solvation structure. Although more bonds are formed between Zn^{2^+} ion and oxygen (O) atoms in $Zn[H_2O]_6^{2^+}$ than in $Zn[H_2O]_5[THF]^{2^+}$, the calculated average bond length in $Zn[H_2O]_6^{2^+}$ (2.06Å based on our DFT calculations) is longer than that in $Zn[H_2O]_5[THF]^{2^+}$ (1.98Å). Furthermore, based on the structures of 6 H_2O / 5 H_2O + 1 THF molecules as shown in **Figure S2**, more hydrogen bonds are broken in the process of forming $Zn[H_2O]_6^{2^+}$, compared to the number of broken bonds in the formation of $Zn[H_2O]_5[THF]^{2^+}$. These two factors could explain why $Zn[H_2O]_5[THF]^{2^+}$ has lower solvation energy than $Zn[H_2O]_6^{2^+}$, which can decrease the water activity.

Figure 1b shows the Raman spectra of the prepared electrolytes and the pure THF solvent. The optimal 2M ZnSO₄/THF 5% shows an inconspicuous difference with baseline 2M ZnSO₄ electrolyte. The distinct peaks of THF disappear when 5% THF additive is added to the 2M ZnSO₄ electrolyte, but the peaks can be observed in 2M ZnSO₄/THF 10%. This finding indicates that a small quantity of THF (less than 10%) can be fully absorbed in the primary solvation shell of Zn²⁺ by the hydrogen bond with H₂O, decreasing the interaction between active H₂O molecules and the Zn²⁺ to restrain the generation of the by-products. This phenomenon was evidenced by the Fourier transform infrared (FTIR) spectroscopy as shown in Figure 1c. In the FTIR spectra profile, the pure THF shows characteristic IR peaks at around 1180, 1065, and 903 cm⁻¹, but these peaks cannot be found when 5% THF was mixed with 2M ZnSO₄ because of the formation between a small amount of THF and H₂O. Therefore, the IR peaks of bare 2M ZnSO₄ and 2M ZnSO₄/THF 5% electrolytes are almost overlapped. Digital images of electrolytes in vials are shown in Figure S3 and Figure 1d. Both 2M ZnSO₄ and 2M ZnSO₄/THF 5% electrolytes are transparent at the initial state, and they keep stable after 30 days. The wettability

of 2M ZnSO₄ and ZnSO₄/THF 5% electrolyte on zinc foil was characterized by the contact angle measurement. As shown in **Figure 1e**, the contact angle of ZnSO₄/THF 5% on the zinc foil is 45°, which is much smaller than that of the baseline 2M ZnSO₄ (79°). The significantly decreased contact angle indicates the remarkably improved surface wettability of the ZnSO₄/THF 5% electrolyte on the zinc foil. The good wettability of ZnSO₄/THF 5% on the zinc foil leads to a more uniform deposition of zinc on the surface of the Zn-metal electrode, achieving and thus favoring the reversible and stable electrochemical behavior.²⁹⁻³⁰

3.2. Electrochemical Performance of Zn||Cu Asymmetrical Cell and Zn Symmetrical Cell

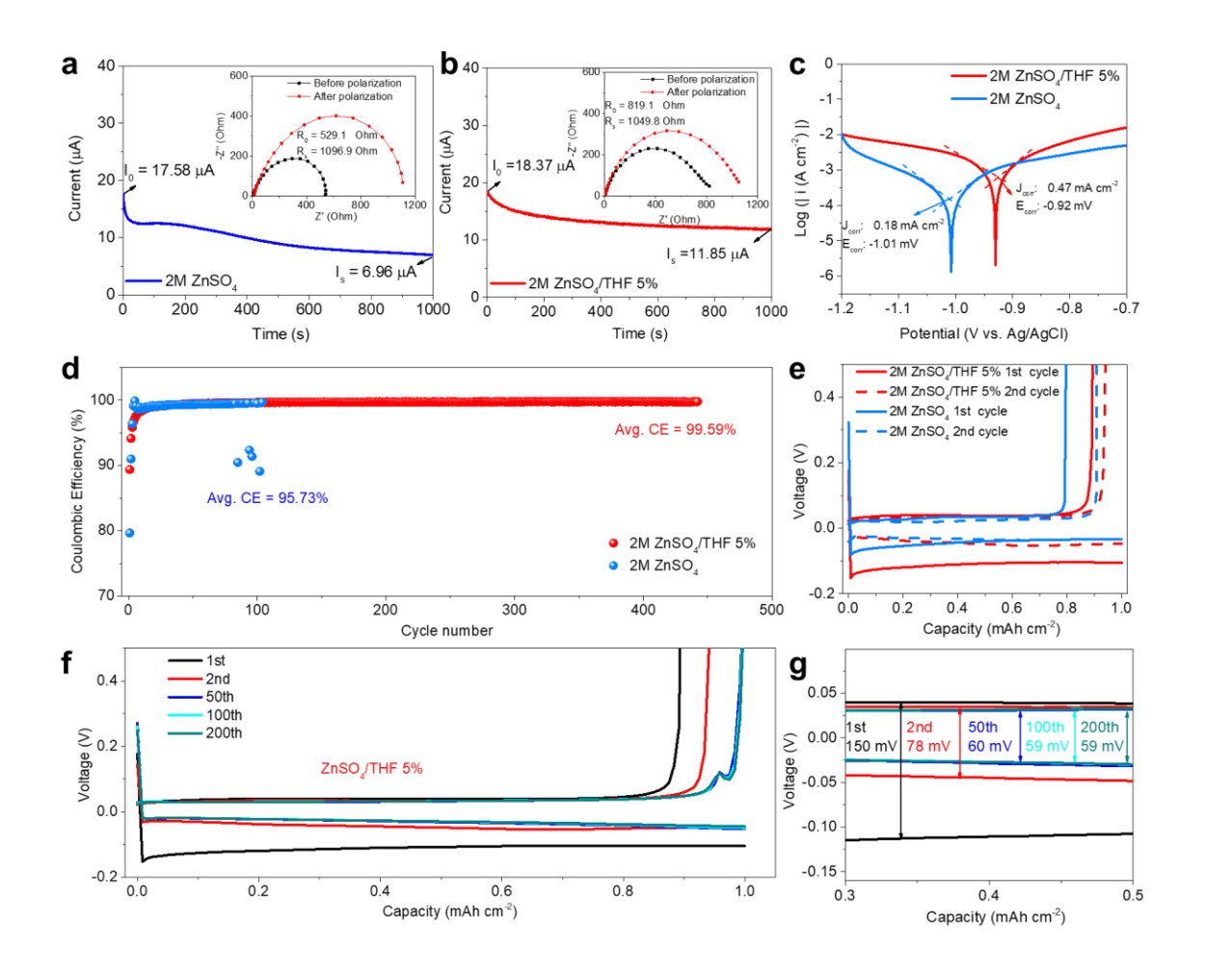


Figure 2. Electrochemical properties of different electrolytes. (a) Current-time plots of Zn symmetric cell with 2M ZnSO₄ electrolyte after the application of a constant potential (25 mV) and the

corresponding impedance spectra before and after polarization; (b) Current-time plots of Zn symmetric cell with ZnSO₄/THF 5% electrolyte after the application of a constant potential (25 mV) and the corresponding impedance spectra before and after polarization. (c) Comparison Tafel plots representing corrosion behavior of Zn electrodes under different electrolyte systems. (d) Zn plating/stripping CE of Zn||Cu cells with different electrolytes. (e) voltage profiles in the 2M ZnSO₄ and 2M ZnSO₄/THF 5% electrolytes at the initial two cycles. (f, g) Voltage profiles of Zn plating/stripping processes at selected cycles in ZnSO₄/THF 5% electrolyte.

The stability of zinc metal anode before battery operation was evaluated by soaking Zn electrodes in different electrolytes for 10 days. Then the Zn chips were measured by the SEM to examine the morphology change of their surface. Figure S4 a-b show the SEM images and the corresponding digital photo of a zinc foil without any treatment. When the zinc chip was immersed in baseline 2M ZnSO4 electrolyte for 10 days, the surface morphology had a sharp change that many particles can be found in the SEM image as shown in Figure S4 c-d, indicating that the baseline 2M ZnSO4 electrolyte can corrode zinc metal anode in a static state, resulting in the precipitation of by-products, as reported. In contrast, after being soaked in 2M ZnSO4/THF 5% electrolyte, the zinc chip kept its surface morphology very well according to the SEM images and digital photograph (Figure S4 e-f), indicating that the THF additive can protect the zinc electrode against the corrosion in the aqueous electrolyte before battery operation.

The electrochemical stability windows of various aqueous electrolytes were evaluated on non-active titanium electrodes. As shown in **Figure S5**, the electrochemical stability window of the baseline 2M ZnSO₄ electrolyte is 2.28 V with a cathode limit of -0.01 V versus Zn²⁺ and an anodic limit of 2.27 V versus Zn²⁺. In contrast, the 2M ZnSO₄/THF 5% electrolyte shows a wider stability window of ~2.38 V. The 2M ZnSO₄/THF 5% was also found to have a slight extent both cathodic (-0.06 V versus Zn²⁺, **Figure S5b**) and anodic (2.32 V versus Zn²⁺, **Figure S5c**) limits.⁴ The transference number of Zn²⁺ (tzn^{2+}) was based on measurements in symmetrical

Zn cells with the help of EIS before and following chronoamperometry (CA) tests and was determined by the following equation:³³⁻³⁴

$$t_{Zn^{2+}} = \frac{I_s(\Delta V - I_0 R_0)}{I_0(\Delta V - I_s R_s)}$$

 ΔV is the applied voltage (25 mV). I_0 and I_s are the initial and steady-state current, where R_0 and R_s are initial and steady-state electrode resistance, respectively.³⁵ The Zn²⁺ transference number of the baseline 2M ZnSO₄ electrolyte is 0.36 based on data from Figure 2a, which is consistent with the references. 36-37 On the other hand, the optimal Zn²⁺ solvation configuration affects the transference number (t_{Zn}^{2+}) in the 2M ZnSO₄/THF 5% electrolyte. As shown in **Figure 2b**, t_{Zn}^{2+} is computed to be 0.51, higher than that for bare 2M ZnSO₄ electrolyte of 0.36, which suggests a faster migration speed of Zn²⁺ in ZnSO₄/THF 5%. ^{13, 36-37} The Tafel plots were obtained by linear polarization measurements to confirm the effect of THF additive on Zn corrosion. From the fitting data in Figure 2c, the corrosion current density of 2M ZnSO₄/THF 5% electrolyte is 0.47 mA cm⁻², which is greater than that of 2M ZnSO₄ with a corrosion current density of 0.18 mA cm⁻². However, the corrosion potential in the 2M ZnSO₄/THF 5% electrolyte increased to -0.92 V from -1.01 V in the baseline 2M ZnSO₄ electrolyte. The much more positive corrosion potential of the 2M ZnSO₄/THF 5% demonstrates less tendency toward corrosion reactions. ³⁸⁻³⁹ The chronoamperometry (CA) was further used to study the effectiveness of THF additive in inhibiting zinc dendrite growth. As shown in Figure S6, the current density with baseline 2M ZnSO₄ electrolyte increases rapidly in the first 50 s and then slowly increases to 250 s, suggesting a propagation of rough Zn deposition. 40-41 In contrast, the 2M ZnSO₄/THF 5% electrolyte displays a steady current from 20 s to 250 s after an increase in current during the initial deposition stage. As a result, the THF additive might prevent Zn²⁺ from moving laterally

(two-dimensional diffusion) by acting as an energy barrier and thereby reducing the tip effect and dendrite formation.

The impact of THF additive on CE of Zn plating/stripping was investigated on Zn||Cu asymmetrical cells. Figure S7 displays the cyclic voltammetry (CV) of Cu working electrodes with a scan rate of 1 mV s⁻¹ at the first cycle. The results indicate that the THF additive increased the overpotential by 40 mV due to the lower ionic conductivity of the 2M ZnSO₄/THF 5% electrolyte. As shown in Figure 2d, the initial CE of Zn||Cu cell at 1 mA cm⁻² and 1 mAh cm⁻² in the 2M ZnSO₄ is 79.65 %, which is lower than that of in the ZnSO₄/THF (5%) electrolyte with a CE value of 89.39 %. The CE values of Zn||Cu cells in these two electrolytes further increase to 99.9 % after 10 cycles and then remain stable and unchanged. For Zn||Cu cell in the 2M ZnSO₄, the CE value starts to fluctuate after 90 cycles and turns to failure just after 100 cycles, which is caused mainly by side reactions and dendritic deposition. An average CE of 95.73 % was obtained in the first 100 cycles. In contrast, Zn||Cu cells with the THF additive displayed a significantly improved Zn plating/stripping reversibility, showing a stable CE after 430 cycles with a high average value of 99.59 %. Figure 2e compares plating/stripping curves of Zn||Cu cells with different electrolytes. In the first cycle, the cell with ZnSO₄/THF 5% electrolyte displayed a higher voltage polarization of 107 mV than that with 2M ZnSO₄ electrolyte (39 mV), consistent with the CV tests. The THF additive increased the overpotential of Zn plating/stripping on the Cu surface due to the decreased ionic conductivity of the electrolyte. In the following second cycle, the overpotential of Zn||Cu cell in ZnSO₄/THF 5% electrolyte reduce to 48 mV, compared to 35 mV of that in 2M ZnSO₄ electrolyte. Figure 2f and Figure 2g show the voltage profiles of Zn plating/stripping on Cu surface at selected cycles in ZnSO₄/THF 5% electrolyte. The curves are almost overlapped in the 50th, 100th, and 200th cycles with a steady

overpotential of 30 mV, suggesting excellent reversibility of Zn metal anode in ZnSO₄/THF 5% electrolyte. The CE of Zn||Cu asymmetrical cell with the ZnSO₄/THF 10% electrolyte is shown in **Figure S8**. An average CE of 98.52 % is obtained over 100 cycles in the ZnSO₄/THF 10% electrolyte, which is higher than that of baseline 2M ZnSO₄ electrolyte (95.73%), but it is lower than that of the optimized ZnSO₄/THF 5% electrolyte (99.59%). Besides, the cell with ZnSO₄/THF 10% electrolyte shows a very high voltage polarization of over 400 mV in the first cycle because of the redundant THF molecules, resulting in the damage of the overall electrochemical performance.

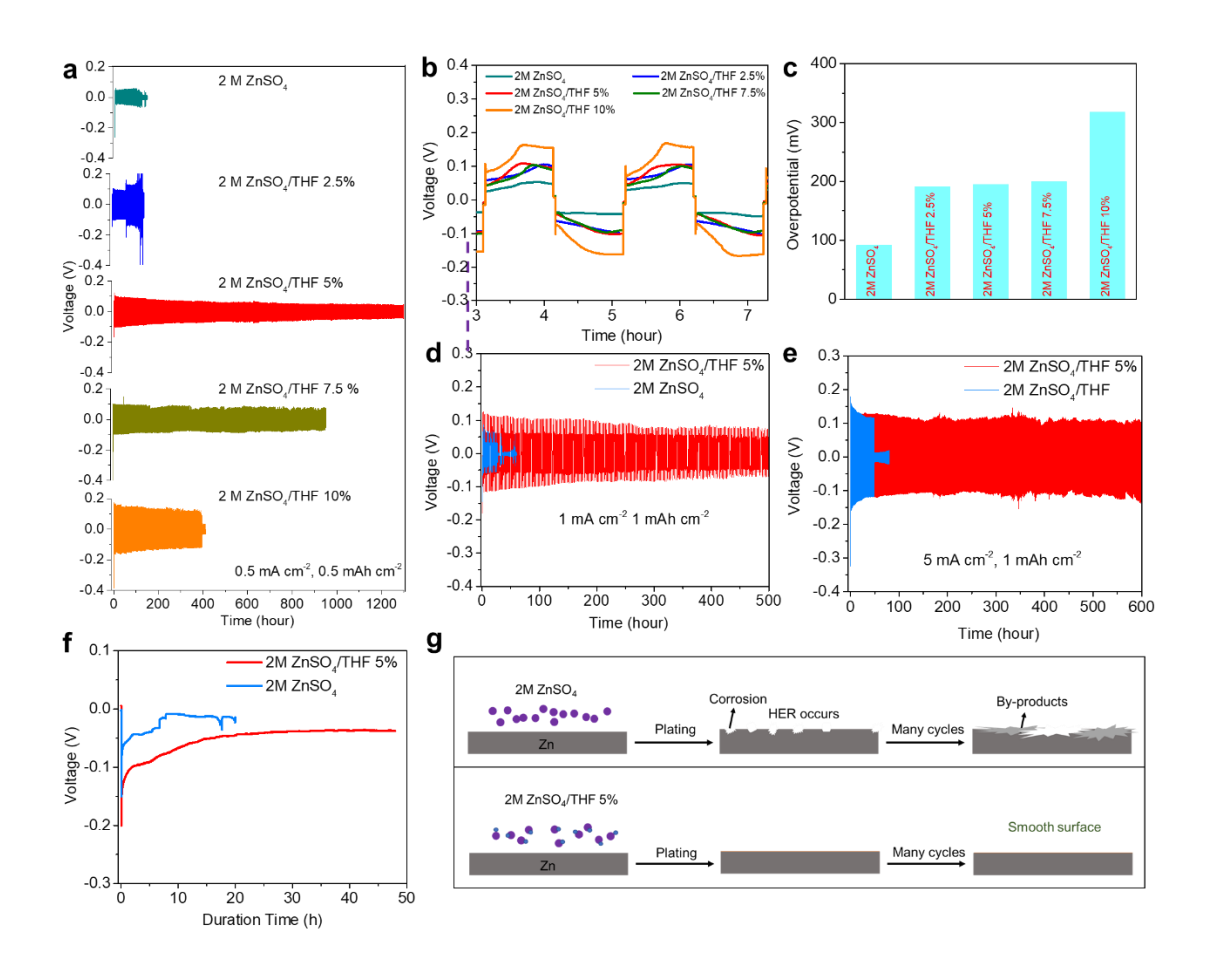


Figure 3. Electrochemical performances of Zn symmetrical cell. (a) Galvanostatic Zn plating/stripping in Zn symmetrical cell at 0.5 mA cm⁻² and 0.5 mAh cm⁻². (b)Voltage profiles of the Zn symmetric cells at 0.5 mA cm⁻² and 0.5 mAh cm⁻². (c) The corresponding overpotential in Zn symmetric cells at 0.5 mA cm⁻².

Galvanostatic Zn plating/stripping in the Zn symmetrical cell at (d) 1 mA cm⁻² and 1 mAh cm⁻² and (e) at 5 mA cm⁻² and 1 mAh cm⁻². (f) Overcharging test of Zn symmetric cells at 1 mA cm⁻². (g) Illustration of surface evolution mechanism with and without THF additive.

To optimize the content of THF in the 2M ZnSO₄ electrolyte, voltage-time profiles of Zn symmetric cells with different electrolytes are shown in Figure 3a. It can be found that the longest plating/stripping cycles were achieved in the presence of 5% THF (by volume) in 2M ZnSO₄ i.e., ZnSO₄/THF 5%. With the addition of THF, the overpotential is larger than that of the baseline 2M ZnSO₄ electrolyte (Figure 3b and 3c). The overpotential rises slightly with an increase of the THF concentration from 2.5% to 7.5% by volume. When the concentration of the THF additive reaches 10%, the overpotential of the Zn symmetric cell surges to more than 300 mV. Thus, 5% is considered the optimal concentration of THF in the 2M ZnSO₄ electrolyte. Further measurements, characterizations, and comparisons were based on the baseline 2M ZnSO₄ and ZnSO₄/THF 5% unless stated. According to Figure 3a and Figure S9, when the cells were tested at a current density of 0.5 mA cm⁻² with a capacity of 0.5 mAh cm⁻², the cell with the 2M ZnSO₄ electrolyte failed after only 120 hours, while it can reach an ultralong cycling life of over 1300 hours with the ZnSO₄/THF 5% electrolyte. Meanwhile, the cell in 2M ZnSO₄ exhibits a stable polarization overpotential of ~ 47 mV at the beginning, which is smaller than that of ZnSO₄/THF 5% (~ 75 mV), and after that, a sudden and irreversible decrease of the polarization voltage appeared, and then the cell failed due to Zn dendrite growth. As a comparison, the overpotential of Zn symmetrical cell in ZnSO₄/THF 5% keeps stable over 1300 hours in Figure **S9d.** The overpotential of the cell with the ZnSO₄/THF 5% electrolyte is larger than that of 2M ZnSO₄, which is attributed to the introduction of THF additive to slightly reduce the ionic conductivity and increase the resistance. The EIS result in Figure S10 confirms that both electrolyte resistance and the charge transfer resistance of 2M ZnSO₄/THF 5% are greater than

that of baseline 2M ZnSO₄, suggesting the decrease of the ionic conductivity by introducing organic THF additive. At a higher current density of 1 mA cm⁻² and a capacity of 1 mAh cm⁻², the cells with 2M ZnSO₄ display inferior cycle stability of only 40 hours and 80 hours (Figure 3d and Figure S11). After introducing a 5% THF additive into the electrolyte, the Zn symmetrical cell can achieve a prolonged cycle life of over 500 hours. The cycling stability of the Zn symmetrical cell in 2M ZnSO₄/THF 5% was further tested under a very high current density of 5 mA cm⁻² with a capacity of 1 mAh cm⁻² (Figure 3e). The result also reveals a great improvement in cycling stability, in which the cell with baseline 2M ZnSO₄ electrolyte lasted for only 60 h while the cell with the 2M ZnSO₄/THF 5% electrolyte showed excellent cycling performance over 600 h. These results show a 10-fold improvement in cycle life at different current densities, demonstrating the THF additive can suppress the side reactions and dendrite growth to boost the cycling stability. In Figure 3f, the overcharge tests of Zn symmetric cells in the 2M ZnSO₄ and ZnSO₄/THF 5% electrolyte were conducted at a current density of 1 mA cm⁻². The discharge capacity of the Zn metal electrode can reach over 48 mAh cm⁻² in ZnSO₄/THF 5%, while that of in the pure 2M ZnSO₄ electrolyte is less than 20 mAh cm⁻² before the cells short-circuited. The excellent overcharge performance reveals that the THF additive has the potential to achieve better reversibility and higher rate capability. The plating/stripping hours of 2M ZnSO₄/THF 5% are compared to the previously reported literature as summarized in **Table S2**. It is found that the THF additive can achieve long plating/stripping performance at various current densities. The excellent cycling stability of the cells with 2M ZnSO₄/THF 5% electrolyte is attributed to the THF additive, which can decrease the water activity to suppress the HER and by-products precipitation. Figure 3g depicts that the Zn electrode can be easily corroded under traditional baseline ZnSO₄ electrolyte upon cycling, while smooth plating of Zn can be achieved

with the existence of THF additive in ZnSO₄ electrolyte. This is because the solvation structure of the Zn hydration layer can be optimized by the THF additive, suppressing the side reactions and dendrite growth during the Zn plating/stripping processes.

3.3. Cycled Zn Electrode Characterization

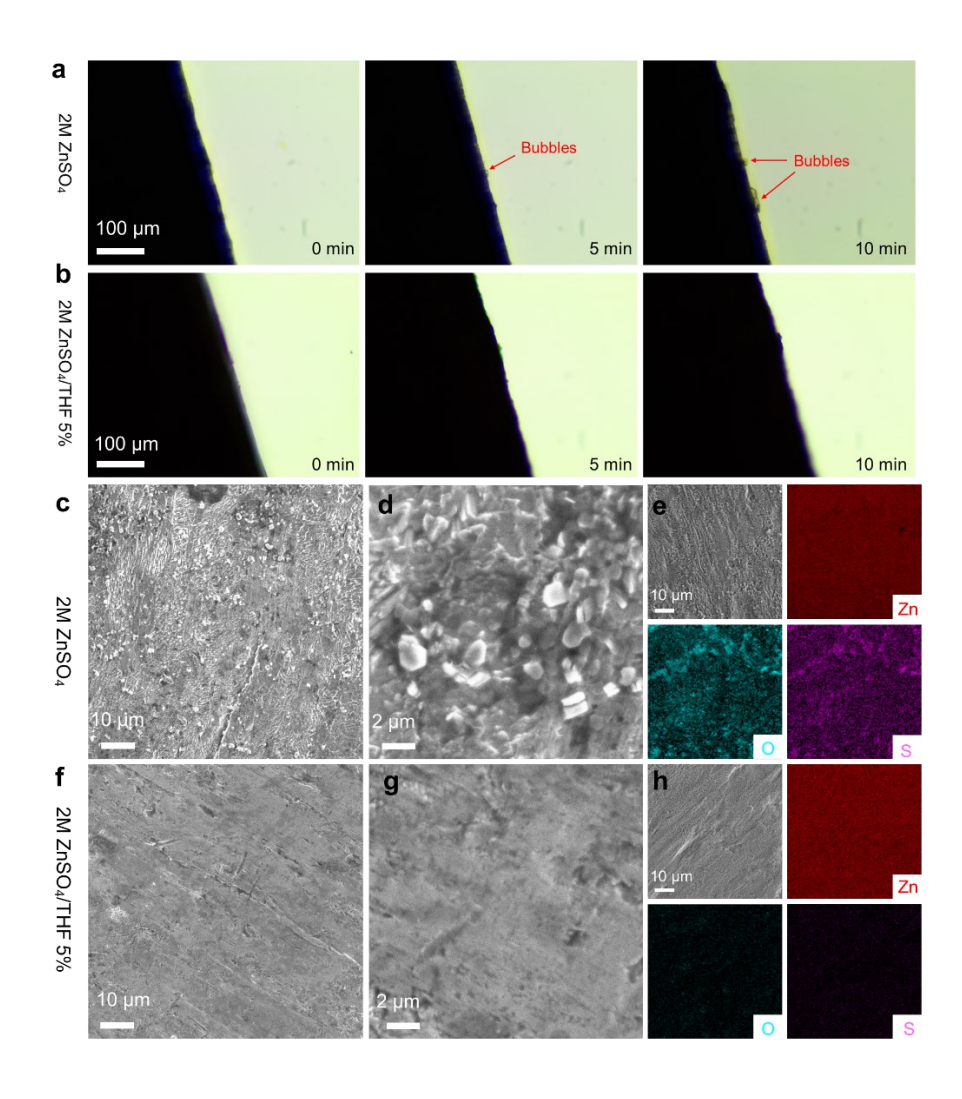


Figure 4. (a, b) *In*-situ optical microscopy of H₂ generation in 2M ZnSO₄ and 2M ZnSO₄/THF 5% in the symmetrical cells at a current density of 10 mA cm⁻². SEM images of (c, d) Zn foil after 100th plating in the 2M ZnSO₄, and (e) corresponding EDS mapping. SEM images of (f, g) Zn foil after 100th plating in the 2M ZnSO₄/THF 5%, and (h) corresponding EDS mapping.

X-ray diffractometer (XRD) was further employed to investigate the crystal structure of zinc foil after Zn deposition. The XRD profiles of bare zinc and zinc foil after plating in 2M ZnSO₄

and ZnSO₄/THF 5% are illustrated in Figure S12. Some new peaks located at 17° and 26° emerged after Zn plating in the baseline 2M ZnSO₄ electrolyte, which is consistent with the Zn₄SO₄(OH)₆·xH₂O.⁴²⁻⁴³ In contrast, with a 5% THF additive in the 2M ZnSO₄ electrolyte, the peaks of by-product Zn₄SO₄(OH)₆·xH₂O disappear in the XRD pattern. Therefore, the THF additive in the ZnSO₄ electrolyte can significantly suppress the generation of by-products of Zn₄SO₄(OH)₆·xH₂O by modulating the solvated structure of the Zn hydration layer. The HER is regarded as an important degradation mechanism of the Zn electrode. The volume expansion comparison after cycles of Zn symmetrical cells with different electrolytes is displayed in Figure S13. The thickness of the coin cell with the baseline 2M ZnSO₄ electrolyte increases from 3.07 cm to 3.32 cm after 100 cycles because of the release of H₂, while there is only a slight increase (3.09 cm to 3.11 cm) of 2M ZnSO₄/THF 5% after 100 cycles. Moreover, a home-built device was developed for *in-situ* monitoring of hydrogen gas evolution (Figure S14). The as-designed cells were tested at a current density of 10 mA cm⁻², where an optical microscope was used to detect the generation of bubbles. As shown in Figure 4a, some bubbles are generated on the surface of the Zn electrode in the baseline 2M ZnSO₄ electrolyte after 5 minutes, and more bubbles are found after 10 minutes. In contrast, the bubbles are barely detected in the electrolyte with the THF additive, indicating the hydrogen gas evolution has been suppressed by the THF additive (**Figure 4b**).

The surface morphologies of Zn foil before and after 100 plating/stripping cycles in the 2M ZnSO₄ and ZnSO₄/THF 5% electrolytes are investigated by photographs and scanning electron microscopy (SEM). Optical images of the Zn electrode after 100 cycles reveal that the surface of the Zn electrode in 2M ZnSO₄ is coarse while it shows a smooth surface in the 2M ZnSO₄/THF 5% electrolyte (**Figure S15**). According to SEM images in **Figure S16**, the surface of zinc electrode

before cycling is smooth with some grooves. After 100 plating/stripping cycles in the baseline 2M ZnSO₄ at a current density of 0.5 mA cm⁻² and a capacity of 0.5 mAh cm⁻², the surface of Zn foil is severely eroded to be quite rough and uneven, as shown in Figure 4c. Besides, many tiny particles of by-products adhere to the surface of the zinc metal electrode (Figure 4d). This structure with erosion surface and "dead Zn" can increase the surface area between the electrode and electrolyte to reduce the CE and capacity of AZMBs, as well as provide more reaction sites for side reactions. The EDS elemental mapping of Zn electrodes after 100 plating/stripping cycles was performed to further investigate the distribution of the elements on the surface (Figure 4e). The EDS mapping finds widespread O and S on the surface of the Zn electrode with 2M ZnSO₄ electrolyte, corresponding to the formation of the by-product of Zn₄SO₄(OH)₆·xH₂O. Once the electrolyte contained a 5% THF additive, the surface of Zn foil became much smoother than that of the baseline 2M ZnSO₄ and is comparable to the original Zn foil morphology (Figure 4f and Figure 4g). According to the EDS mapping in Figure 4h, it can be observed that the Zn element covers the whole surface with 2M ZnSO₄/THF 5% electrolyte, while little O and S can be detected. These results have successfully proven that the THF additive can inhibit side reactions including HER and by-products precipitation because of the decrease in water activity.

3.4. Full Cell Evaluation

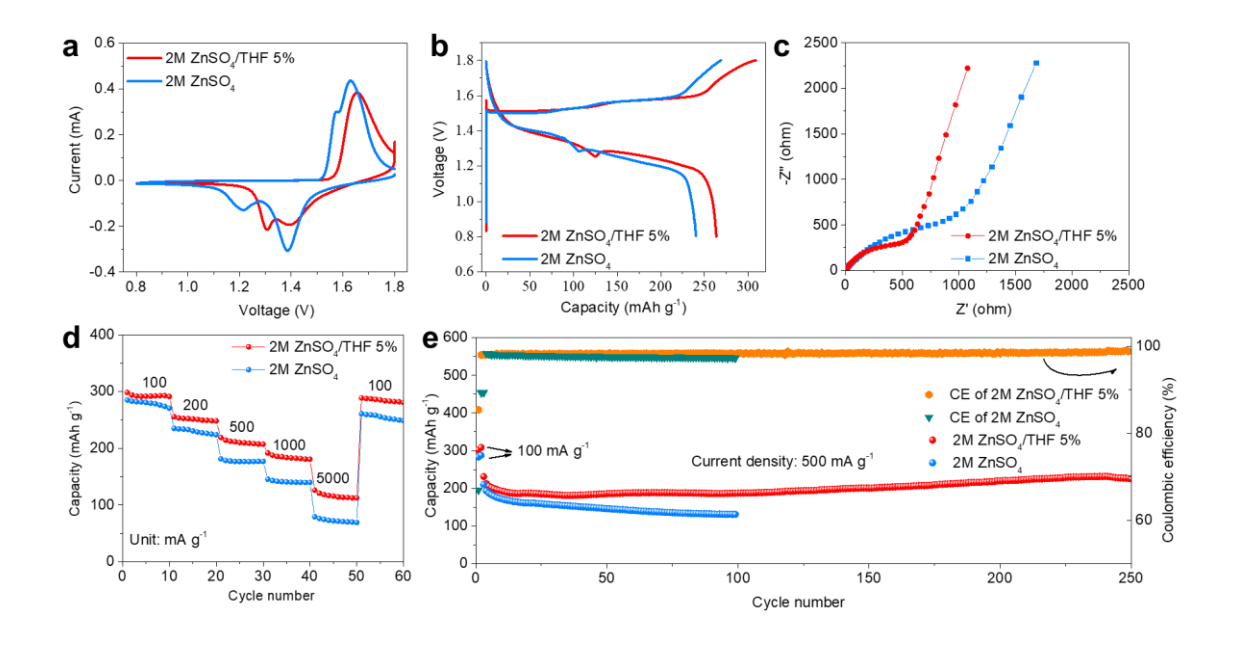


Figure 5. Electrochemical performance of Zn||MnO₂ cells in different electrolytes. (a) CV at a scan rate of 0.1 mV s⁻¹. (b) Charge-discharge profiles. (c) EIS spectra. (d) Rate performance. (e) Cyclic stability at 500 mA g⁻¹.

To evaluate the practical application of ZnSO₄/THF 5% electrolyte, the full cell with Zn as anode and the β-MnO₂ as the cathode (a tunnel structure) was assembled and tested. MnO₂ is one of the most promising cathodes for AZMBs due to its high theoretical capacity of 308 mAh g⁻¹.44-45 To address the issue of the dissolution loss of MnO₂ active material upon cycling, the MnSO₄ salt was added to the electrolytes with a concentration of 0.1 M. **Figure 5a** shows the CV curves of the Zn||MnO₂ cells in 2M ZnSO₄ and ZnSO₄/THF 5% electrolytes at a scan rate of 0.1 mV s⁻¹. The MnO₂ electrode in different electrolytes shows similar behavior with distinct Mn-ion redox peaks. A smaller overpotential gap is observed in the CV curve for the ZnSO₄/THF 5% electrolyte compared with that using 2M ZnSO₄ electrolyte, which is consistent with voltage profiles of galvanostatic charge/discharge as shown in **Figure 5b**. The cell with the ZnSO₄/THF 5% electrolyte also shows a smaller charge-transfer resistance (R_{ct}) than that of the

baseline 2M ZnSO₄ electrolyte (Figure 5c). This maybe because the THF organic additive promote the infiltration of the electrolyte into the MnO₂ electrode, as well as wetting the MnO₂ active material with PVDF binder. Figure 5d shows the rate performance of different electrolytes at various current densities from 100 mA g⁻¹ to 5000 mA g⁻¹. The result shows that cells with different electrolytes deliver similar capacities at a low current density of 100 mA g⁻¹, but the cell with THF additive shows higher capacities than that of the baseline 2M ZnSO₄ electrolyte with the increase of the current densities. The cycling properties of the Zn||MnO₂ cell were tested at a current density of 500 mA g⁻¹ after the activation at a small current density of 100 mA g⁻¹ for the initial two cycles. As shown in Figure 5e, the MnO₂ cathode in ZnSO₄/THF 5% electrolyte delivers a capacity of 225.2 mAh g⁻¹ after 250 cycles, decreasing from 231.3 mAh g⁻¹ in the 3rd cycle with a capacity retention of 97.56%. The capacity of Zn||MnO₂ batteries with 2M ZnSO₄/THF 5% electrolytes is on the rise from the 50th cycle to the 240th cycle because of the addition of MnSO₄ and THF. The MnSO₄ can provide the additional Mn^{2+} ions in the electrolytes, which would be electrochemically oxidized to MnO_x on the MnO_2 electrode to provide additional capacity. Meanwhile, the THF additive shows the capability of decreasing the water activity, which may be able to prevent the dissolution loss of MnO₂. By comparison, the MnO₂ cathode in baseline 2M ZnSO₄ electrolyte exhibits inferior cycling stability that the capacity decreases dramatically to 130.8 mAh g⁻¹ after 100 cycles with a capacity retention of 62.05%. Figure S17 shows the 1st, 2nd, 10th, 50th, and 100th capacityvoltage profiles of the full cell with Zn metal electrode in ZnSO₄/THF 5% electrolyte. The curves of 10th, 50th, and 100th nearly overlapped, revealing that the Zn metal anode has a stable and reversible electrochemical behavior in ZnSO₄/THF 5% electrolyte. This full cell result shows the proof of concept and the promise for practical application.

4. Conclusion

A common and low-cost cyclic ether of THF was introduced into the 2M ZnSO₄ electrolyte. The THF as a proton acceptor can form a hydrogen bond with H₂O, thus it can optimize the solvation structure of the Zn hydration layer to decrease the water activity. The water-induced undesired reactions are therefore suppressed, which can improve the electrochemical behavior of zinc metal anode with good cycle stability and high Columbic efficiency. The Zn plating/stripping tests confirm that 5% THF (by volume) is considered as the optimal concentration in the 2M ZnSO₄ electrolyte. The Zn symmetrical cell in ZnSO₄/THF 5% electrolyte exhibits an ultralong cycle life of more than 1300 hours at 0.5 mA cm⁻² with a capacity of 0.5 mAh cm⁻². According to the *ex-situ* SEM images, the surface of Zn foil became much smoother after plating/stripping cycling in ZnSO₄/THF 5% electrolyte than that in baseline 2M ZnSO₄. The THF additive also enables a high Coulombic efficiency in Zn||Cu cells with an average value of 99.59% over 430 cycles. The MnO₂ cathode in Zn||MnO₂ full cell with ZnSO₄/THF 5% electrolyte delivers a high reversible capacity of 225 mAh g⁻¹ after 250 cycles with a capacity retention of 97.56%.

Supporting Information

The supporting information is available free of charge at http://pubs.acs.org.

Details of the DFT calculation, chemical structures, and home-built cell for *in-situ* monitoring of hydrogen gas evolution. Additional characterization of the electrolyte and electrode (digital photos, SEM images, and XRD pattern). Supplementary electrochemical analysis and battery performance (CV curves, LSV curves, CA curves, discharge-charge profiles, and EIS spectra).

Acknowledgments

This work was partially supported by the National Science Foundation under awards CBET-2038082 and CBET-2038083. We also acknowledge the support from EDA University Center Program (ED18DEN3030025).

Conflict of Interest

The authors declare no financial/commercial conflicts of interest.

Reference

- 1. Yang, H.; Qiao, Y.; Chang, Z.; Deng, H.; Zhu, X.; Zhu, R.; Xiong, Z.; He, P.; Zhou, H., Reducing Water Activity by Zeolite Molecular Sieve Membrane for Long-Life Rechargeable Zinc Battery. *Advanced Materials* **2021**, *33* (38), 2102415.
- 2. Ma, L.; Chen, S.; Li, N.; Liu, Z.; Tang, Z.; Zapien, J. A.; Chen, S.; Fan, J.; Zhi, C., Hydrogen-Free and Dendrite-Free All-Solid-State Zn-Ion Batteries. *Advanced Materials* **2020**, *32* (14), 1908121.
- 3. Wang, F.; Borodin, O.; Gao, T.; Fan, X.; Sun, W.; Han, F.; Faraone, A.; Dura, J. A.; Xu, K.; Wang, C., Highly Reversible Zinc Metal Anode for Aqueous Batteries. *Nature Materials* **2018**, *17* (6), 543-549.
- 4. Cao, L.; Li, D.; Pollard, T.; Deng, T.; Zhang, B.; Yang, C.; Chen, L.; Vatamanu, J.; Hu, E.; Hourwitz, M. J.; Ma, L.; Ding, M.; Li, Q.; Hou, S.; Gaskell, K.; Fourkas, J. T.; Yang, X.-Q.; Xu, K.; Borodin, O.; Wang, C., Fluorinated Interphase Enables Reversible Aqueous Zinc Battery Chemistries. *Nature Nanotechnology* **2021**, *16* (8), 902-910.

- 5. Sun, W.; Wang, F.; Zhang, B.; Zhang, M.; Küpers, V.; Ji, X.; Theile, C.; Bieker, P.; Xu, K.; Wang, C.; Winter, M., A Rechargeable Zinc-Air Battery Based on Zinc Peroxide Chemistry. *Science* **2021**, *371* (6524), 46-51.
- 6. Chen, Z.; Mo, F.; Wang, T.; Yang, Q.; Huang, Z.; Wang, D.; Liang, G.; Chen, A.; Li, Q.; Guo, Y.; Li, X.; Fan, J.; Zhi, C., Zinc/Selenium Conversion Battery: A System Highly Compatible with Both Organic and Aqueous Electrolytes. *Energy & Environmental Science* **2021**, *14* (4), 2441-2450.
- 7. He, W.; Chen, K.; Pathak, R.; Hummel, M.; Lamsal, B. S.; Gu, Z.; Kharel, P.; Wu, J. J.; Zhou, Y., Achieving High Pseudocapacitance Anode by An *In Situ* Nanocrystallization Strategy for Ultrastable Sodium-Ion Batteries. *ACS Applied Materials & Interfaces* **2021**, *13* (19), 22577-22585.
- 8. He, W.; Chen, K.; Pathak, R.; Hummel, M.; Reza, K. M.; Ghimire, N.; Pokharel, J.; Lu, S.; Gu, Z.; Qiao, Q.; Zhou, Y., High-Mass-Loading Sn-Based Anode Boosted by Pseudocapacitance for Long-Life Sodium-Ion Batteries. *Chemical Engineering Journal* **2021**, 414, 128638.
- 9. Liu, C.; Luo, Z.; Deng, W.; Wei, W.; Chen, L.; Pan, A.; Ma, J.; Wang, C.; Zhu, L.; Xie, L.; Cao, X.-Y.; Hu, J.; Zou, G.; Hou, H.; Ji, X., Liquid Alloy Interlayer for Aqueous Zinc-Ion Battery. *ACS Energy Letters* **2021**, *6* (2), 675-683.
- 10. Cao, Z.; Zhu, X.; Xu, D.; Dong, P.; Chee, M. O. L.; Li, X.; Zhu, K.; Ye, M.; Shen, J., Eliminating Zn Dendrites by Commercial Cyanoacrylate Adhesive for Zinc Ion Battery. *Energy Storage Materials* **2021**, *36*, 132-138.

- 11. Zhou, J.; Xie, M.; Wu, F.; Mei, Y.; Hao, Y.; Huang, R.; Wei, G.; Liu, A.; Li, L.; Chen, R., Ultrathin Surface Coating of Nitrogen-Doped Graphene Enables Stable Zinc Anodes for Aqueous Zinc-Ion Batteries. *Advanced Materials* **2021**, *33* (33), 2101649.
- 12. Wang, M.; Zhang, F.; Lee, C.-S.; Tang, Y., Low-Cost Metallic Anode Materials for High Performance Rechargeable Batteries. *Advanced Energy Materials* **2017**, *7* (23), 1700536.
- 13. Hao, J.; Yuan, L.; Ye, C.; Chao, D.; Davey, K.; Guo, Z.; Qiao, S.-Z., Boosting Zinc Electrode Reversibility in Aqueous Electrolytes by Using Low-Cost Antisolvents. *Angewandte Chemie International Edition* **2021**, *60* (13), 7366-7375.
- 14. Cao, L.; Li, D.; Hu, E.; Xu, J.; Deng, T.; Ma, L.; Wang, Y.; Yang, X.-Q.; Wang, C., Solvation Structure Design for Aqueous Zn Metal Batteries. *Journal of the American Chemical Society* **2020**, *142* (51), 21404-21409.
- 15. Liu, S.; Mao, J.; Pang, W. K.; Vongsvivut, J.; Zeng, X.; Thomsen, L.; Wang, Y.; Liu, J.; Li, D.; Guo, Z., Tuning the Electrolyte Solvation Structure to Suppress Cathode Dissolution, Water Reactivity, and Zn Dendrite Growth in Zinc Ion Batteries. *Advanced Functional Materials* **2021**, *31* (38), 2104281.
- 16. Zhang, Q.; Ma, Y.; Lu, Y.; Zhou, X.; Lin, L.; Li, L.; Yan, Z.; Zhao, Q.; Zhang, K.; Chen, J., Designing Anion-Type Water-Free Zn²⁺ Solvation Structure for Robust Zn Metal Anode. *Angewandte Chemie* **2021**, *133* (43), 23545-23552.
- 17. Zhang, C.; Shin, W.; Zhu, L.; Chen, C.; Neuefeind, J. C.; Xu, Y.; Allec, S. I.; Liu, C.; Wei, Z.; Daniyar, A.; Jiang, J.-X.; Fang, C.; Alex Greaney, P.; Ji, X., The Electrolyte Comprising More Robust Water and Superhalides Transforms Zn-Metal Anode Reversibly and Dendrite-Free. *Carbon Energy* **2021**, *3* (2), 339-348.

- 18. Zhang, Q.; Ma, Y.; Lu, Y.; Li, L.; Wan, F.; Zhang, K.; Chen, J., Modulating Electrolyte Structure for Ultralow Temperature Aqueous Zinc Batteries. *Nature Communications* **2020**, *11* (1), 4463.
- 19. Cai, S.; Chu, X.; Liu, C.; Lai, H.; Chen, H.; Jiang, Y.; Guo, F.; Xu, Z.; Wang, C.; Gao, C., Water–Salt Oligomers Enable Supersoluble Electrolytes for High-Performance Aqueous Batteries. *Advanced Materials* **2021**, *33* (13), 2007470.
- 20. Sun, P.; Ma, L.; Zhou, W.; Qiu, M.; Wang, Z.; Chao, D.; Mai, W., Simultaneous Regulation on Solvation Shell and Electrode Interface for Dendrite-Free Zn Ion Batteries Achieved by a Low-Cost Glucose Additive. *Angewandte Chemie International Edition* **2021**, *60* (33), 18247-18255.
- 21. Shi, J.; Xia, K.; Liu, L.; Liu, C.; Zhang, Q.; Li, L.; Zhou, X.; Liang, J.; Tao, Z., Ultrahigh Coulombic Efficiency and Long-Life Aqueous Zn Anodes Enabled by Electrolyte Additive of Acetonitrile. *Electrochimica Acta* **2020**, *358*, 136937.
- 22. Xu, W.; Zhao, K.; Huo, W.; Wang, Y.; Yao, G.; Gu, X.; Cheng, H.; Mai, L.; Hu, C.; Wang, X., Diethyl Ether as Self-Healing Electrolyte Additive Enabled Long-Life Rechargeable Aqueous Zinc Ion Batteries. *Nano Energy* **2019**, *62*, 275-281.
- 23. Pham, T. D.; Bin Faheem, A.; Lee, K.-K., Design of a LiF-Rich Solid Electrolyte Interphase Layer through Highly Concentrated LiFSI–THF Electrolyte for Stable Lithium Metal Batteries. *Small* **2021**, *17* (46), 2103375.
- 24. Takamuku, T.; Nakamizo, A.; Tabata, M.; Yoshida, K.; Yamaguchi, T.; Otomo, T., Large-Angle X-Ray Scattering, Small-Angle Neutron Scattering, and Nmr Relaxation Studies on Mixing States of 1,4-Dioxane-Water, 1,3-Dioxane-Water, and Tetrahydrofuran-Water Mixtures. *Journal of Molecular Liquids* **2003**, *103-104*, 143-159.

- 25. Gutmann, V.; Gutmann, V., *The Donor-Acceptor Approach to Molecular Interactions*. Springer: 1978; Vol. 228.
- 26. Mhin, B. J.; Lee, S.; Cho, S. J.; Lee, K.; Kim, K. S., Zn(H₂O)₂₊⁶ Is Very Stable among Aqua-Zn(II) ions. *Chemical Physics Letters* **1992**, *197* (1), 77-80.
- 27. Dong, Y.; Miao, L.; Ma, G.; Di, S.; Wang, Y.; Wang, L.; Xu, J.; Zhang, N., Non-Concentrated Aqueous Electrolytes with Organic Solvent Additives for Stable Zinc Batteries. *Chemical Science* **2021**, *12* (16), 5843-5852.
- 28. De, S.; Ali, S. M.; Ali, A.; Gaikar, V. G., Micro-Solvation of The Zn²⁺ Ion–A Case Study. *Physical Chemistry Chemical Physics* **2009**, *11* (37), 8285-8294.
- 29. Pathak, R.; Chen, K.; Gurung, A.; Reza, K. M.; Bahrami, B.; Pokharel, J.; Baniya, A.; He, W.; Wu, F.; Zhou, Y.; Xu, K.; Qiao, Q., Fluorinated Hybrid Solid-Electrolyte-Interphase for Dendrite-Free Lithium Deposition. *Nature Communications* **2020**, *11* (1), 93.
- 30. Chen, K.; Pathak, R.; Gurung, A.; Reza, K. M.; Ghimire, N.; Pokharel, J.; Baniya, A.; He, W.; Wu, J. J.; Qiao, Q.; Zhou, Y., A Copper-Clad Lithiophilic Current Collector for Dendrite-Free Lithium Metal Anodes. *Journal of Materials Chemistry A* **2020**, *8* (4), 1911-1919.
- 31. Hao, J.; Yuan, L.; Zhu, Y.; Jaroniec, M.; Qiao, S.-Z., Triple-Function Electrolyte Regulation toward Advanced Aqueous Zn-Ion Batteries. *Advanced Materials* **2022**, *34* (44), 2206963.
- 32. Hao, J.; Long, J.; Li, B.; Li, X.; Zhang, S.; Yang, F.; Zeng, X.; Yang, Z.; Pang, W. K.; Guo, Z., Toward High-Performance Hybrid Zn-Based Batteries via Deeply Understanding Their Mechanism and Using Electrolyte Additive. *Advanced Functional Materials* **2019**, *29* (34), 1903605.

- 33. Xing, Z.; Xu, G.; Xie, X.; Chen, M.; Lu, B.; Zhou, J.; Liang, S., Highly Reversible Zinc-Ion Battery Enabled by Suppressing Vanadium Dissolution Through Inorganic Zn²⁺ Conductor Electrolyte. *Nano Energy* **2021**, *90*, 106621.
- 34. Wang, Y.; Fan, Y.; Liao, D.; Wu, Y.; Yu, Y.; Hu, C., Highly Zn²⁺-Conductive and Robust Modified Montmorillonite Protective Layer of Electrodes toward High-Performance Rechargeable Zinc-Ion Batteries. *Energy Storage Materials* **2022**, *51*, 212-222.
- 35. Yan, H.; Li, S.; Nan, Y.; Yang, S.; Li, B., Ultrafast Zinc–Ion–Conductor Interface toward High-Rate and Stable Zinc Metal Batteries. *Advanced Energy Materials* **2021**, *11* (18), 2100186.
- 36. Park, J. H.; Kwak, M.-J.; Hwang, C.; Kang, K.-N.; Liu, N.; Jang, J.-H.; Grzybowski, B. A., Self-Assembling Films of Covalent Organic Frameworks Enable Long-Term, Efficient Cycling of Zinc-Ion Batteries. *Advanced Materials* **2021**, *33* (34), 2101726.
- 37. Hao, J.; Li, X.; Zhang, S.; Yang, F.; Zeng, X.; Zhang, S.; Bo, G.; Wang, C.; Guo, Z., Designing Dendrite-Free Zinc Anodes for Advanced Aqueous Zinc Batteries. *Advanced Functional Materials* **2020**, *30* (30), 2001263.
- 38. Chamoun, M.; Hertzberg, B. J.; Gupta, T.; Davies, D.; Bhadra, S.; Van Tassell, B.; Erdonmez, C.; Steingart, D. A., Hyper-Dendritic Nanoporous Zinc Foam Anodes. *NPG Asia Materials* **2015**, *7* (4), e178-e178.
- 39. Jiao, Y.; Li, F.; Jin, X.; Lei, Q.; Li, L.; Wang, L.; Ye, T.; He, E.; Wang, J.; Chen, H.; Lu, J.; Gao, R.; Li, Q.; Jiang, C.; Li, J.; He, G.; Liao, M.; Zhang, H.; Parkin, I. P.; Peng, H.; Zhang, Y., Engineering Polymer Glue towards 90% Zinc Utilization for 1000 Hours to Make High-Performance Zn-Ion Batteries. *Advanced Functional Materials* **2021**, *31* (49), 2107652.
- 40. Xie, S.; Li, Y.; Dong, L., Stable Anode-Free Zinc-Ion Batteries Enabled by Alloy Network-Modulated Zinc Deposition Interface. *Journal of Energy Chemistry* **2023**, *76*, 32-40.

- 41. Xie, S.; Li, Y.; Li, X.; Zhou, Y.; Dang, Z.; Rong, J.; Dong, L., Stable Zinc Anodes Enabled by Zincophilic Cu Nanowire Networks. *Nano-Micro Letters* **2022**, *14* (1), 39.
- 42. Lu, W.; Zhang, C.; Zhang, H.; Li, X., Anode for Zinc-Based Batteries: Challenges, Strategies, and Prospects. *ACS Energy Letters* **2021**, *6* (8), 2765-2785.
- 43. Zhang, G.; Wu, T.; Zhou, H.; Jin, H.; Liu, K.; Luo, Y.; Jiang, H.; Huang, K.; Huang, L.; Zhou, J., Rich Alkali Ions Preintercalated Vanadium Oxides for Durable and Fast Zinc-Ion Storage. *ACS Energy Letters* **2021**, *6* (6), 2111-2120.
- 44. Zhao, Y.; Ma, L.; Zhu, Y.; Qin, P.; Li, H.; Mo, F.; Wang, D.; Liang, G.; Yang, Q.; Liu, W.; Zhi, C., Inhibiting Grain Pulverization and Sulfur Dissolution of Bismuth Sulfide by Ionic Liquid Enhanced Poly(3,4-ethylenedioxythiophene):Poly(styrenesulfonate) for High-Performance Zinc-Ion Batteries. *ACS Nano* **2019**, *13* (6), 7270-7280.
- 45. Li, D.; Cao, L.; Deng, T.; Liu, S.; Wang, C., Design of a Solid Electrolyte Interphase for Aqueous Zn Batteries. *Angewandte Chemie International Edition* **2021**, *60* (23), 13035-13041.

For Table of Contents Only

